Observer based feedback control of 3rd order LCC resonant converters

M. P. Foster, C. M. Bingham, D. A. Stone, H. I. Sewell.
Department of Electronic and Electrical Engineering
University of Sheffield, Mappin Street,
Sheffield, S1 3JD, UK.
Tel. +44 (0) 114 2225195, Fax. +44 (0) 114 2225196
c.bingham@sheffield.ac.uk
www.shef.ac.uk/eee/emd

Keywords

Converter control, DC Power Supply, Estimation techniques, Resonant converters

Abstract

The paper considers specific issues related to the design and realisation of observer-based feedback of isolated output voltage for resonant power converters. To provide a focus to the study, a 3rd order LCC converter is employed as a candidate topology. It is shown that whilst resonant converters nominally operate at high switching frequencies to facilitate the use of small reactive components, by appropriate pre-conditioning of non-isolated resonant-tank voltages and currents, the resulting observer can be implemented at relatively low sampling frequencies, and hence, take advantage of low-cost digital hardware.

Experimental results are used to demonstrate the accuracy of observer estimates under both transient and steady-state operating conditions, and to show operation of the observer as part of a closed-loop feedback system where the LCC resonant converter is used as a regulated power supply.

Introduction

Ideally, the output voltage of a power converter is directly measured and employed within a feedback control-loop to provide a regulated output that is independent of load and/or primary supply voltage. However, for reasons of safety and electromagnetic compatibility/interference suppression, some form of signal isolation between the sensed converter output, and control circuitry, is normally required, which can constitute a significant proportion of the component and production costs.

To overcome these disadvantages, some authors have considered employing state-observers to estimate the (nominally) isolated output of a converter, from a model of the dominant system dynamics, and measurements of (nominally) non-isolated voltages and currents. One such technique, presented in [1], uses an observer to estimate the inductor current from inductor voltage for incorporation within a current mode control loop, for a buck converter. In this particular application using an observer was advantageous as the measured inductor voltage was significantly larger signal than the output of a current-sense resistor.

A feature of the observers used in such converters, is that their dynamics are assumed to have much greater bandwidth than the dominant dynamics of the converter and input/load disturbances. In this way, the observer output can be directly employed as part of a closed-loop feedback system designed to accommodate the effects of exogenous disturbances without the dynamics of the observer contributing significantly to the resulting closed-loop system dynamics. The dominant output dynamics of classical, hard-switched converter topologies viz. with series and parallel LC output filters, are, for the most part, governed by the time constant of the output filter, with the average values of the non-isolated voltages and currents being employed for the calculation of observer estimates. This has significant practical advantages for the digital implementation of the observer

since comparatively low sample rates can be adopted, thereby facilitating the use of low cost of digital processing hardware.

For use in resonant converters, however, where high switching frequencies (typically 100kHz to 2.6MHz) are employed to excite a tank circuit (often with high Q) close to its resonant frequency, to facilitate low-loss switching of the power devices, the (nominally) non-isolated voltages and currents of interest for use in observer calculations, vary sinusoidally at the switching frequency. Moreover, it is often the peak values of the resonant voltages and currents that dictate the output voltage of the converter, thus precluding the use of simple, low-cost averaging circuitry employed when implementing observers with other, hard-switched, converter counterparts.

Here then, the paper considers the design of digital observers for estimating the output voltage of resonant converters based on the envelope detection of resonant-tank voltages and currents. Although the resonant variables oscillate at high frequency, their envelopes change with relatively low bandwidth, thus necessitating relatively low observer sampling rates, and facilitates the use of low-cost processing hardware normally associated with hard-switched converter counterparts. Although the presented methodology is ultimately applicable to all resonant converter types, a 3rd order LCC variant is considered here to provide a focus to the study.

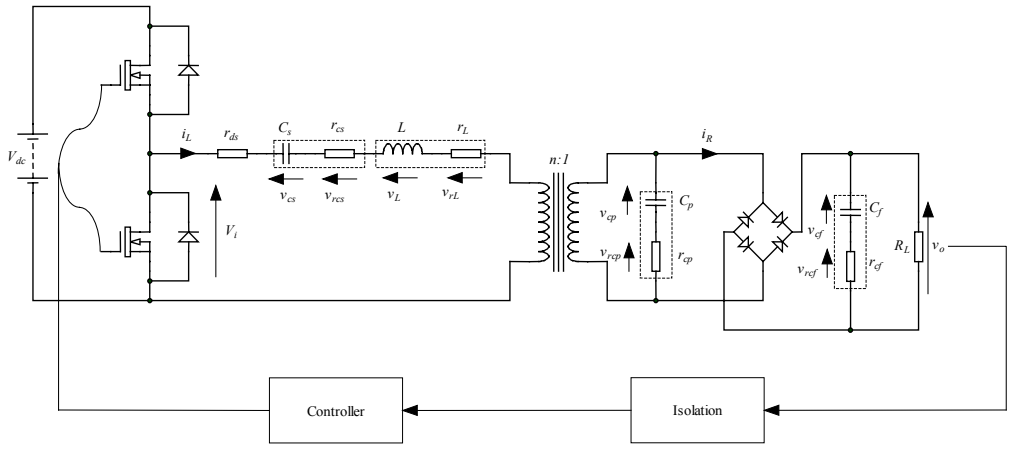

(a)

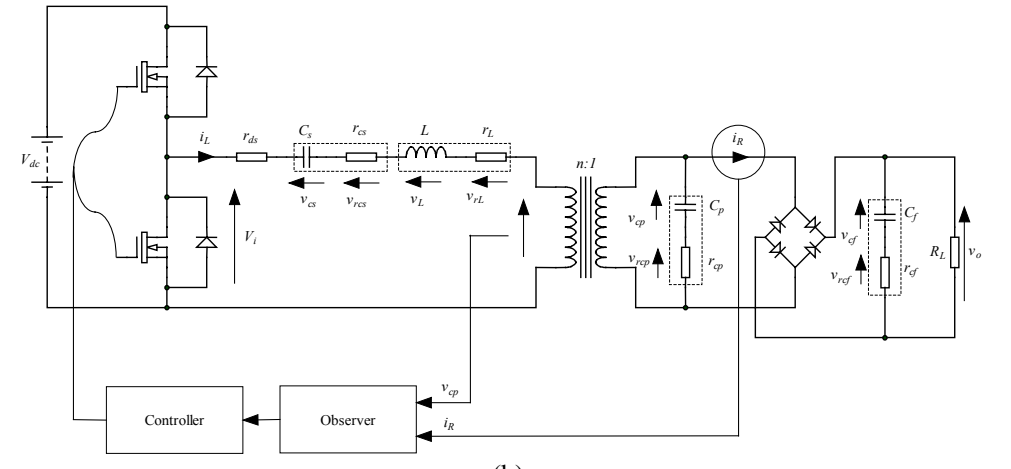

(b)

Fig. 1: LCC voltage-output converter (a) isolated output feedback,
(b) feedback of output voltage from observer

Operation of LCC voltage-output resonant converters

Figure 1 shows a schematic of a 3rd order LCC voltage output resonant converter that will be used as a basis for the derivation and realisation of Luenberger observers. The series (C_s) and parallel (C_p) capacitors, the resonant inductor (L) and filter capacitor (C_f), are augmented with parasitic resistances for completeness, as these are known to have significant influence on circuit operation. The power switches are used to excite the resonant tank just above the resonant frequency to facilitate zero voltage switching, allowing high operating frequencies (typically >>100kHz) to be employed with a corresponding reduction in the size of reactive components.

The dynamic characteristics of the converter can be conveniently analysed by partitioning the circuit into fast and slow sub-systems and developing the related coupling equations [4]. The fast sub-system is associated with the resonant circuit and the slow sub-system typically models the output filter and load. An additional coupling equation describes the interaction of the rectifier with the output filter and the resonant circuit. For brevity, the model given in (1), however, the reader is directed to the account given in [2] for full derivation details. Note that, for simplicity the transformer turns ratio, n, is assumed to be 1:1. Also, the magnetising inductance of the transformer is assumed to have only a minor influence on the behaviour of this converter.

$$\begin{bmatrix} \dot{v}_{Cp} \\ \dot{v}_{Cs} \\ \dot{i}_L \\ \dot{v}_{Cf} \end{bmatrix} = \begin{bmatrix} 0 & 0 & \frac{1}{C_p} & 0 \\ 0 & 0 & \frac{1}{C_s} & 0 \\ -\frac{1}{L} & -\frac{1}{L} & -\frac{r_{ds}+r_{Cs}+r_{Cp}+r_L}{L} & 0 \\ 0 & 0 & 0 & -\frac{1}{C_f\left(R_L+r_{Cf}\right)} \end{bmatrix} \begin{bmatrix} v_{Cp} \\ v_{Cs} \\ i_L \\ v_{Cf} \end{bmatrix} + \begin{bmatrix} -\frac{i_R}{C_p} \\ 0 \\ \frac{V_i}{L}+\frac{i_R r_{Cp}}{L} \\ \frac{|i_R| R_L}{C_f\left(R_L+r_{Cf}\right)} \end{bmatrix}$$

$$i_R = \begin{cases} \frac{C_f}{C_f+C_p} i_L + \operatorname{sgn}(i_L) \frac{C_p}{R_L\left(C_f+C_p\right)} v_{Cf} & |v_{cp}| > v_{Cf} + 2V_d \\ 0 & |v_{cp}| \le v_{Cf} + 2V_d \end{cases} \quad (1)$$

For efficient operation the converter is assumed to be operating above resonance, [3]. In this case, 6 distinct operating modes (M1 to M6) exist in each switching cycle of the input voltage, defined with respect to the polarity of the input voltage and the state of the rectifier current. Figure 2 shows example voltage (current) waveforms across (through) various components in the circuit during steady-state operation.

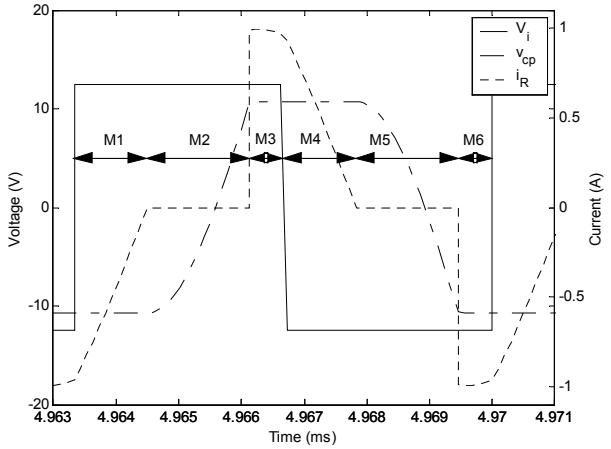

Mode 1: V_i>0, i_R < 0 - (M1)

Mode 2: V_i>0, i_R = 0 - (M2)

Mode 3: V_i>0, i_R >0 - (M3)

Mode 4: V_i<0, i_R > 0 - (M4)

Mode 5: V_i<0, i_R = 0 - (M5)

Mode 6: V_i<0, i_R < 0 - (M6)

Fig. 2: Voltages and currents of a 3rd order voltage output LCC resonant converter

The circuit enters operating Mode 1 (M1) when the input voltage changes polarity from negative to positive. At this time $i_R<0$, and that the rectifier is conducting. Throughout M1 the parallel capacitor voltage v_{cp} is clamped to the output voltage due to the action of the bridge rectifier. When the rectifier current crosses zero, the bridge rectifier switches off and the converter enters M2. During M2, the output filter is essentially 'disconnected' from the resonant circuit and the parallel capacitor voltage begins to charge from the negative supply rail, towards the positive supply rail. At the time when $v_{cp}= v_{cf}+2V_d$, the bridge rectifier again begins to conduct (M3) and v_{cp} is clamped to v_{cf}. Due to symmetrical operation of this circuit in steady-state, modes M4, M5 and M6 are analogous to modes M1, M2 and M3 with voltage and current polarities reversed. From (1) it can be seen that the output voltage of the converter is essentially given by the voltage across C_f (ignoring parasitic effects), which, in turn, is governed by the magnitude of the rectifier current, $|i_R|$, and the current drawn by the load:

$$\frac{dv_{Cf}}{dt} = \frac{|i_R|}{C_f} - \frac{v_{Cf}}{C_f R_L} \qquad (2)$$

Consulting fig. 2, it can be seen that during modes M1, M3, M4 and M6, v_{cp} is clamped to v_{cf} via the action of the bridge rectifier. The magnitude (peak-value) of v_{cp} therefore provides a convenient variable for input to an observer (not forgetting to allow for the rectifier on state voltage drop), whose design is based on the converter dynamics given by (2).

State estimation

The basis of most state-variable estimation (observer) techniques is to generate an 'error' signal, formed by subtracting measured system output(s) from the estimated observer output(s), and, by implementing a feedback mechanism, drive the error towards zero. In general, the designer has the freedom to select the bandwidth of the observer convergence dynamics, although, in reality, the preferred use of digital implementation means that sampling rate limitations imposed by A/D converter performance, and finite word-length effects, often constrain design freedom.

The general structure of a traditional (Luenberger [7]) observer suitable for linear systems is shown in fig. 3, where, in this case, *y(t)* are the system outputs and *u(t)* are the system inputs. As discussed previously, the output of the system, *y(t)*, is compared with the output of a dynamic model of the system, $\tilde{y}(t)$, resulting in an error $e_y(t)$. The error signal is then used to correct for modelling inaccuracies via the observer gain matrix, *L*. Eqn.(3) describes the state variable model of the system, and the state-variable description of the observer, and clearly shows the action of the error correction mechanism. The design of *L* is specified by considering the error, $e_x(t)$, between the actual system state, *x(t)*, and the observed state, $\tilde{x}(t)$, also given in (3). To make the error converge independently of the state, *x(t)*, and input, *u(t)*, the observer dynamics, and input, matrices should, respectively, be chosen as $\tilde{A} = A - LC$, and $\tilde{B} = B$, the former also notably governing the error convergence dynamics by appropriate assignment of the eigenvalues of $\tilde{A} = A - LC$ using the degrees of freedom given by *L*.

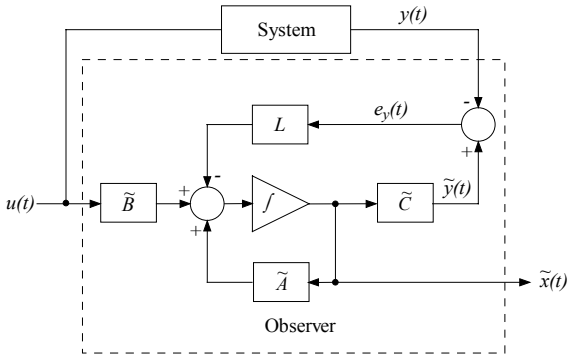

Fig. 3: Classical Luenberger observer for linear systems

$$\begin{aligned}
\dot{x}(t) &= Ax(t) + Bu(t) && \text{system dynamics} \\
\dot{\tilde{x}}(t) &= \tilde{A}\tilde{x}(t) + \tilde{B}u(t) - Le_y && \text{observer dynamics} \\
\dot{e}_x(t) &= \tilde{A}e_x(t) + \left(A - LC - \tilde{A}\right)x(t) + \left(B - \tilde{B}\right)u(t) && \text{error dynamics}
\end{aligned} \tag{3}$$

where $x(t)$ – system state-variables
$u(t)$ – system inputs
$y(t)$ – system outputs
$\tilde{x}(t)$ – observer state-variables
A,B,C and $\tilde{A},\tilde{B},\tilde{C}$ – appropriately dimensioned dynamics, input and output matrices
L – observer gain matrix

The preference to implement observer schemes in digital hardware requires discretisation of the system dynamics of (3). The step-invariant transform yields,

$$\begin{aligned}
x[k+1] &= e^{A\Delta T}x[k] + A^{-1}(e^{A\Delta T} - I)Bu[k] \\
&= Fx[k] + Gu[k]
\end{aligned} \tag{4}$$

where $F = e^{A\Delta T}, G = A^{-1}(e^{A\Delta T} - I)B$ and ΔT is the sample period for observer implementation.

Similarly, the structure of the corresponding observer is given by,

$$\tilde{x}[k+1] = \tilde{F}\tilde{x}[k] + \tilde{G}u[k] + \tilde{H}y[k] \tag{5}$$

where $\tilde{F} = e^{(\tilde{A}-L\tilde{C})\Delta T}, \tilde{G} = (\tilde{A} - L\tilde{C})^{-1}(e^{(\tilde{A}-L\tilde{C})\Delta T} - I)\tilde{B}, \tilde{H} = (\tilde{A} - L\tilde{C})^{-1}(e^{(\tilde{A}-L\tilde{C})\Delta T} - I)L$ (6)

The observer gain, L, is chosen to achieve a bandwidth from the observer that is K times higher than the required system dynamics. For this particular application, the observer gain, L, is chosen such that the eigenvalues of the observer, λ_{obs}, are K-times closer to the centre of the unit circle than the discretised output-filter dynamics, λ_{conv}:

$$\begin{aligned}
&\lambda_{conv} = e^{\frac{-\Delta T}{C_f R_L}}, \lambda_{obs} = e^{\left(\frac{-1}{C_f R_L} - L\right)\Delta T} \\
&\lambda_{obs} = \frac{1}{K}\lambda_{conv} \\
&\therefore L = \frac{1}{\Delta T}\ln(K)
\end{aligned} \tag{7}$$

Substituting L into (5) leads to the finalised discrete-time observer,

$$\begin{aligned}
\tilde{v}_{Cf}(k+1) = {} & \frac{1}{K}e^{\frac{-\Delta T}{C_f R_L}}\tilde{v}_{Cf}[k] - \frac{R_L}{1 + \Delta T C_f R_L \ln(K)}\left(\frac{1}{K}e^{\frac{-\Delta T}{C_f R_L}} - 1\right)\left|i_R[k]\right| \\
& - \frac{C_f R_L \ln(K)}{\Delta T\left(1 + C_f R_L \ln(K)\right)}\left(\frac{1}{K}e^{\frac{-\Delta T}{C_f R_L}} - 1\right)\left|\hat{v}_{Cp}[k]\right|
\end{aligned} \tag{8}$$

To correctly implement (8), the converter voltages/currents must be sampled at a high rate, at least twice the switching frequency to correctly capture all the resonant circuit dynamics. However, it can be see from (2) that the output filter dynamics are of a much lower bandwidth than the resonant circuit. In general, due to the relatively large time constant of the filter capacitor and load, with respect to the response time of the resonant circuit, it can be seen, fig. 4, that the output filter responds to the average value rectifier input current, i_R. Figure 4 shows the correlation between the average

rectifier input current and the output current (both measured with a LEM PR50 50MHz current probe) for the prototype converter. Therefore, it is proposed to low-pass filter (average) the input signal to allow the sample period, ΔT, to be reduced for implementation

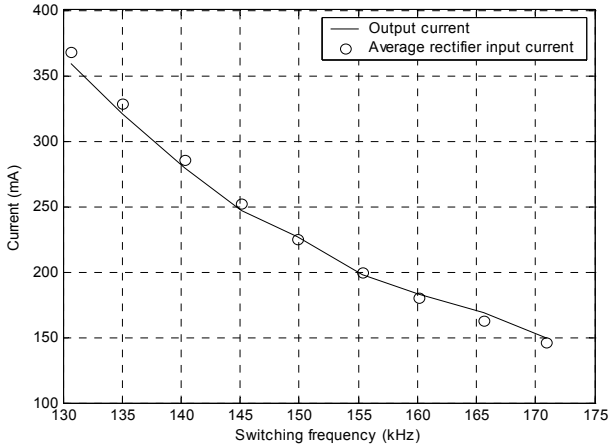

Fig. 4: Correlation between the average output current and the average rectifier input current

To satisfy the Nyquist sampling criterion, the sample period should be chosen to be a least 2× faster than the maximum frequency of interest. The sample period, ΔT, can be chosen using the following equation to relate to the time constant of the output filter with the observer gain and to satisfy the sampling criterion,

$$\Delta T = \frac{C_f R_L}{K_{Nyquist} K_{obs}} \tag{9}$$

where $K_{Nyquist}$ represents the over sampling rate and K_{obs} is the number of times faster the observer poles are required to be, with respect to the poles output filter.

Observer Implementation

Figure 5 shows the underlying structure of the resulting observer-based scheme for estimating the output voltage, including the additional, low-cost, interface requirements to obtain the dynamic envelopes of v_{cp} and i_R.

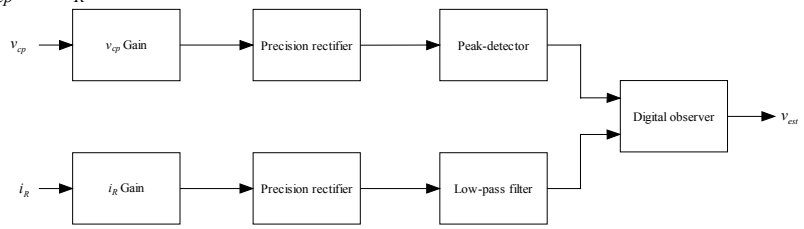

Fig. 5: Block diagram of observer

A prototype 25V input, 5W, LCC resonant converter is used to demonstrate the design, realisation and performance of the proposed observer scheme. Specific component values of the converter are given in Table I. The reader is directed to [2,5,6] for design and analysis methods suitable for this converter topology.

Here, the precision rectifiers are made from Analog Devices AD8036 clamping operational amplifiers, and the peak-detector for sensing the parallel capacitor voltage is based on a simple op-amp/diode based peak-detector using the LM6361. The average value of rectifier current is

determined from a simple 1st-order low-pass filter with a corner frequency of 1.6kHz. The discrete-time observer and resulting closed-loop controller are implemented on a Microchip PIC18F452.

Input Voltage	V_i	25V
Parallel Tank Capacitor	C_p	47nF
Series Tank Capacitor	C_s	47nF
Tank Inductor	L	50μH
Output Filter Capacitor	C_f	1000μF
Nominal Resonant frequency	f_0	≈130kHz
Transformer turns ratio	n	1
Output Load	R_L	25Ω

Table I: Component values of prototype LCC resonant converter

From (8), the estimated output voltage is calculated from (10) noting that $\left|\hat{v}_{Cp}[k]\right|$ is the sampled sequence of peak values of parallel capacitor voltage and $\left|i_{R\_av}[k]\right|$ is the sampled sequence of averaged rectifier input current values.

$$\tilde{v}_{Cf}[k+1] = \alpha\tilde{v}_{Cf}[k] + \beta\left|i_{R\_av}[k]\right| + \gamma\left|\hat{v}_{Cp}[k]\right| \tag{10}$$

where $\alpha = \frac{1}{K}e^{\frac{-\Delta T}{C_f R_L}}, \beta = -\frac{R_L}{1+\Delta T C_f R_L \ln(K)}\left(\frac{1}{K}e^{\frac{-\Delta T}{C_f R_L}} - 1\right), \gamma = -\frac{C_f R_L \ln(K)}{\Delta T\left(1+\Delta T C_f R_L \ln(K)\right)}\left(\frac{1}{K}e^{\frac{-\Delta T}{C_f R_L}} - 1\right)$

Here, the sample period is $\Delta T = 155\mu s$, giving α=0.4969, β=0.1115, γ=0.4986. The observer gain term, L, is chosen to assign the eigenvalue at λ=0.4969.

Experimental Results

Open-loop operation of the observer-converter system under transient start-up conditions, for a range of operating frequencies, f_s=130,150,170kHz, is given in fig. 6, clearly showing a high degree of correlation exists between both the measured output voltage and estimated output voltage from the observer.

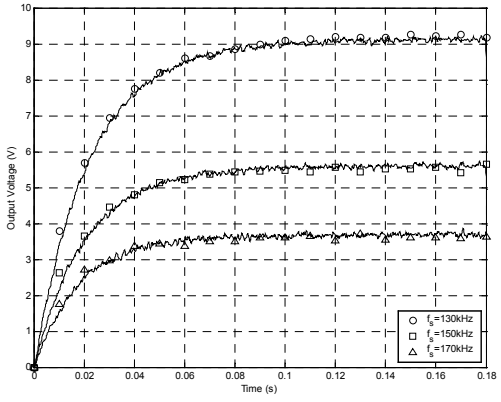

Fig. 6: Transient start-up data from observer (O,□Δ) and measured (-) output voltage

To demonstrate observer accuracy over a wide operating envelope, the measured and estimated (observed) steady-state output voltage are compared in fig. 7 for various switching frequencies and load conditions. Once again, a good correspondence is evident, with a degree of robustness also exhibited.

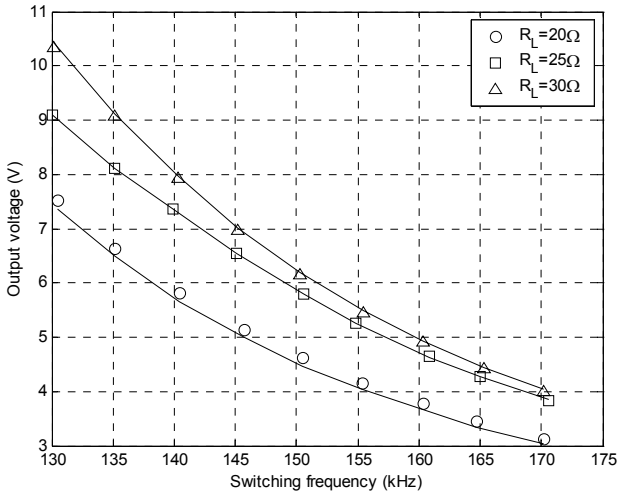

Fig. 7: Frequency response of the discrete-time observer

Closed-loop control

Since the observer has been shown to adequately estimate the output voltage, it can be employed as part of a feedback control system to facilitate the use of the converter as a regulated power supply. Here, the desired reference for the supply is taken to be 5V. Formally, by virtue of the *separation principle*, the design of the controller can be considered independently of the observer, and a structure based on Proportional and Integral (PI) action is adopted, and implemented in the microcontroller. Although many methodologies could be employed for the design of the compensator, here, the proportional controller parameter, $K_p=100$, was chosen to provide a good transient response without causing controller instability and integral gain, $K_i=200$, chosen to reduce steady-state error with sufficient bandwidth to accommodate load changes.

Operation of the supply in closed-loop is demonstrated in fig. 8, which shows the transient response to a step change in output voltage demand from 2.75V to 5V with different DC-link voltages. It is seen that controller exhibits a classic second-order type response with an initial overshoot of 2% which settles to 5V in around 50µs.

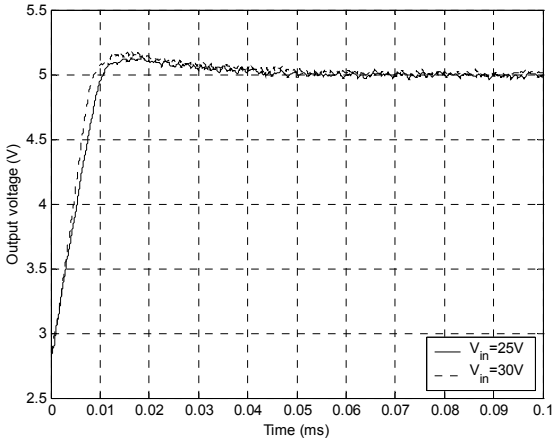

Fig. 8: Response of controller to a step change in reference from 2.75V to 5V

 ISBN : 90-75815-07-7

Conclusions

The paper has addressed specific problems associated with the design and realisation of observer-based output estimation schemes for the isolated operation of resonant converters. By appropriate processing of non-isolated variables of interest, it is shown that linear, discrete-time domain asymptotic observers can be readily employed as an integral part of closed-loop, regulated, resonant power supply. A 3rd order LCC voltage-output converter is used as a candidate topology to demonstrate the attributes of the proposed techniques.

It is shown, that, whilst resonant converters nominally operate at high-switching frequencies, a digital observer can be implemented using relatively low sampling frequencies by using the peak (envelope) and average values of non-isolated voltage and currents.

Comparisons of experimental results with those from the observer show the discrete-time observer can provide accurate predictions of output voltage under both steady-state and transient operating conditions. Additionally, the discrete-time observer has been shown to be successfully incorporated within a feedback control system with experimental results demonstrating the operation of the LCC converter as a regulated power supply.

References

[1]. P. Midya, P. T. Krein, and M. F. Greuel, Sensorless current mode control - An observer-based technique for DC-DC converters, IEEE Trans Power Electronics, vol.16, no. 4, p. 522 –526, July 2001

[2]. M. P. Foster, H. I. Sewell, C. M. Bingham and D. A. Stone, State-variable modelling of LCC voltage output converters, IEE Electronic Letters, (17), p. 1065-1066, 2001.

[3].R. L. Steigerwald, A Comparison of Half-Bridge Resonant Converter Topologies, IEEE Trans. Power Electronics, vol. 3, no. 2, p.174-182, April 1988.

[4]. J. Sun and H. Grotstollen. Symbolic Analysis of Switching Power Converters Based on a General Averaging Method, PESC 96 Record 27th IEEE Power Electronics Specialist Conference, vol. 1, p. 543-549, 1996.

[5]. J. G. Hayes and M. G. Egan, Rectifier-compensated fundamental mode approximation analysis of the series-parallel LCLC family of resonant converters with capacitative output filter and voltage-source load, PESC 99 Record, 30th IEEE Power Electronics Specialist Conference, 1999, Charleston – USA, p.1030-1036.

[6]. A. K. S. Bhat, Analysis and design of a series-parallel resonant converter with capacitive output filter, IEEE Transactions on Industry Applications, vol. 27, No. 3, pp. 523-530, May/June 1991.

[7]. D. G. Luenberger, An Introduction to Observers, IEEE Trans. Automatic Control, vol. AC-16, no. 6, p. 190-197, December 1971.